Equation of state and radii of finite nuclei in the presence of a diffuse surface layer

V. M. Kolomietz, S. V. Lukyanov, A. I. Sanzhur, and S. Shlomo

Phys. Rev. C **95**, 054305 — Published 8 May 2017

DOI: 10.1103/PhysRevC.95.054305

Equation of state and radii of finite nuclei in presence of diffuse surface layer

V.M. Kolomietz[1)], S.V. Lukyanov[1)], A.I. Sanzhur[1)]
and
S. Shlomo[2,3)]

[1)]Institute for Nuclear Research, 03680 Kiev, Ukraine

[2)]Cyclotron Institute, Texas A&M University, College Station, Texas 77843, USA

[3)]Department of Elementary Particles and Astrophysics, the Weizmann Institute of Science, Rehovot 76100, Israel

The definition of nuclear surface and nuclear radii is considered within Gibbs-Tolman-Widom (GTW) approach. We demonstrate the non-monotonic behavior of the nuclear equimolar radii which is due to the shell effects in the chemical potential of finite nuclei. The direct variational method within the extended Thomas-Fermi approximation is used to establish the equation of state for finite nuclei. We have studied the influence of the polarization effect caused by the neutron excess on the particle density and the nuclear radii. This effect increases with the asymmetry parameter X and can be responsible for the appearance of a large neutron halo in nuclei well away from the beta stability line. We have performed new calculations of the A-dependence of the radii $R(A)$ of nucleon distribution which are based on the use the experimental data for the nuclear binding energy. We demonstrate the presence of the quantum shell effects in $R(A)$. We have analyzed the value of the neutron-skin thickness Δr_{np} in the isotopes of the Na, Sn and Pb nuclei within the GTW approach and show the appearance of non-monotonic behavior of Δr_{np} as a function of the neutron excess. We discuss the relative contributions to the neutron-skin thickness Δr_{np} from the skin and the halo effects.

PACS: 24.10.Cn, 21.60.Ev, 24.10.Nz, 24.30.Cz, 24.75+i

I. INTRUDUCTION

The nucleon distribution in finite nuclei possess a surface diffuse layer which occurs due to the quantum penetration of particles into the classically forbidden region. This fact creates the problem of the unambiguous definition of the nuclear surface and thereby of the nuclear size [1]. In particular, a strict definition of the nuclear surface and volume is needed to derive the surface tension σ, the incompressibility coefficient K, etc. Moreover, in a small finite system like a nucleus, the derivation of the equation of state (EOS) meets also some difficulties because of the uncertainty for the pressure in a system with finite surface layer. In a classical liquid, the problem of the proper derivation of the surface of the finite drop in presence of diffuse interface was studied by Gibbs-Tolman-Widom (GTW) [2,3,4] where the concept of the equimolar dividing surface was used.

In the present paper we will apply the classical GTW approach to the nucleus as a quantum liquid drop focusing on the presence of the diffusive surface of the nucleon spatial distribution. The averaged characteristic of nucleon distribution is given by the root mean square (rms) radii for neutron and proton, respectively. Evaluating the values of rms radii and the corresponding neutron-skin thickness, we adopt the extended Thomas-Fermi (ETF) and the direct variational method [5,6]. The nucleon densities $\rho_p(r)$ and $\rho_n(r)$ are generated by the profile functions which are determined by the requirement that the energy of the nucleus should be stationary with respect to variations of these profiles. The GTW concept is employed by the introducing a dividing surface into the profile functions. We study also the problems of the nucleon redistribution within the surface region (nuclear periphery), in particular, the neutron coat and the neutron excess for nuclei far away from the beta stability line as well as the influence of the skin and halo effects on the value of the neutron-skin thickness.

This paper is an extension of our previous work [7] where the general equimolar GTW concept was adopted for nuclei with finite surface layer. In present paper we apply the GTW approach to realistically determine the EOS for finite nuclei and some nuclear characteristics such as the nuclear size, the surface tension, the pressure, etc. Taking into consideration the presence of finite diffuse interface and applying the GTW approach, we redefine the surface and symmetry energies. The use of the GTW approach allows us to present a more realistic procedure for the extraction of the nuclear surface tension coefficient from the experimental data. In contrast to the previous work [7], we avoid the leptodermous approximation and improve the evaluation of the Coulomb energy taking into consideration the finite diffuse layer of the proton distribution. Following the GTW equimolar concept, we derive the curvature as well as the halo and skin

effects on the surface energy and the surface component of symmetry energy.

This paper is organized as follows. In section II we adopt the GTW model of equimolar dividing surface for the two-component liquid drop with finite surface layer. The application of GTW model to some nuclear problems is considered in sections III, IV and V. We conclude and summarize in section VI.

II. EXTENSION OF GIBBS-TOLMAN-WIDOM CONCEPT TO FINITE NUCLEI

Considering a nucleus which possess the finite surface diffuse layer, we will follow the GTW concept of the equimolar dividing surface. We introduce the formal dividing surface of radius R, the corresponding volume $\mathcal{V} = 4\pi R^3/3$ and the surface area $\mathcal{S} = 4\pi R^2$. The dividing surface is arbitrary but located within the nuclear diffuse layer. The energy of a nucleus E, as well as its mass number $A = N + Z$ and the neutron excess $A_- = N - Z$, are split into the volume (bulk) and surface parts,

$$E = E_{\text{bulk}} + E_{\mathcal{S}} + E_C, \quad A = A_{\mathcal{V}} + A_{\mathcal{S}}, \quad A_- = A_{-,\mathcal{V}} + A_{-,\mathcal{S}}. \tag{1}$$

Here the Coulomb energy E_C is fixed and does not depend on the dividing radius R. The bulk energy E_{bulk} is identified with the energy E_∞ of the homogeneous nuclear matter:

$$E_{\text{bulk}} = E_\infty \tag{2}$$

and $E_{\mathcal{S}}$ is the surface energy [4,8]

$$E_{\mathcal{S}} = \left(\sigma + \mu\rho_{\mathcal{S}} + \mu_-\rho_{-,\mathcal{S}}\right)\mathcal{S}, \tag{3}$$

with σ being the surface tension coefficient. The considered nuclear matter is two-component one with isotopic asymmetry $X = (N - Z)/(N + Z)$ and chemical potentials

$$\left.\frac{\partial E_{\text{bulk}}}{\partial N}\right|_{\mathcal{V},Z} = \mu_n, \quad \left.\frac{\partial E_{\text{bulk}}}{\partial N}\right|_{\mathcal{V},N} = \mu_p, \tag{4}$$

where n and p refer to a neutron and a proton, respectively.

The central assumption of the Gibbs-Tolman-Widom approach is that the nuclear matter inside the specified volume $\mathcal{V}$ is chosen to have the chemical potentials μ_n and μ_p equal to the experimental values λ_n and λ_p of the corresponding nucleus, see also [9]:

$$\mu_n(\rho_n, \rho_p) = \lambda_n - \lambda_{n,C}, \quad \mu_p(\rho_n, \rho_p) = \lambda_p - \lambda_{p,C}, \tag{5}$$

where ρ_n and ρ_p are the r-independent bulk densities of neutrons and protons, respectively. The Coulomb contribution $\lambda_{q,C}$ to the nucleon chemical potential λ_q is subtracted in Eq. (5) because the derivation of μ_q in Eq. (4) is written for an uncharged nuclear matter. Here,

$$\lambda_{n,C} = \left.\frac{\partial E_C}{\partial N}\right|_Z, \quad \lambda_{p,C} = \left.\frac{\partial E_C}{\partial Z}\right|_N. \tag{6}$$

We will also use the isoscalar, $\mu = (\mu_n + \mu_p)/2$, and isovector, $\mu_- = (\mu_n - \mu_p)/2$, chemical potentials and the corresponding densities $\rho = \rho_n + \rho_p$ and $\rho_- = \rho_n - \rho_p$. In agreement with the definition of the dividing surface adopted above, both densities ρ and ρ_- include the volume and surface parts

$$\rho_{\mathcal{V}} = A_{\mathcal{V}}/\mathcal{V}, \ \rho_{-,\mathcal{V}} = A_{-,\mathcal{V}}/\mathcal{V} \ \text{ and } \ \rho_{\mathcal{S}} = A_{\mathcal{S}}/\mathcal{S}, \quad \rho_{-,\mathcal{S}} = A_{-,\mathcal{S}}/\mathcal{S}. \tag{7}$$

The bulk energy E_{bulk} in Eqs. (2) and (4) can be evaluated using the Skyrme effective nucleon-nucleon (NN) interaction for the nuclear matter

$$E_{\text{bulk}} = \int d\,\boldsymbol{r}\ \epsilon_{\text{tot}}(\boldsymbol{r}) \equiv \int d\,\boldsymbol{r}\ \epsilon_{\text{tot}}[\rho_n(\boldsymbol{r}), \rho_p(\boldsymbol{r})] \tag{8}$$

The total energy density functional (EDF) of a nuclear matter $\epsilon_{\text{tot}}[\rho_n, \rho_p]$ in Eq. (8) includes the kinetic energy density, $\epsilon_{\text{kin}}[\rho_n, \rho_p]$, the potential energy density associated with Skyrme interaction, $\epsilon_{\text{Sk}}[\rho_n, \rho_p]$

$$\epsilon_{\text{tot}}[\rho_n, \rho_p] = \epsilon_{\text{kin}}[\rho_n, \rho_p] + \epsilon_{\text{Sk}}[\rho_n, \rho_p]. \tag{9}$$

Considering an asymmetric nuclear matter with $X \ll 1$, the bulk energy per particle can be written as [5],

$$E_{\text{bulk}}/A \equiv e_0(\rho) \ + e_2(\rho)\left(\frac{\rho_-}{\rho}\right)^2, \tag{10}$$

where

$$\begin{aligned} e_0 \ = & \frac{\hbar^2}{2m}\alpha\rho^{2/3} + \frac{3t_0}{8}\rho + \frac{t_3}{16}\rho^{\nu+1} \\ & + \frac{\alpha}{16}[3t_1 + t_2(5 + 4x_2)]\rho^{5/3} \end{aligned} \tag{11}$$

and

$$\begin{aligned} e_2 = & \frac{5}{9}\frac{\hbar^2}{2m}\alpha\rho^{2/3} - \frac{t_0}{8}(1 + 2x_0)\rho - \frac{t_3}{48}(1 + 2x_3)\rho^{\nu+1} \\ & + \frac{5\alpha}{72}(t_2(4 + 5x_2) - 3t_1x_1)\rho^{5/3}. \end{aligned} \tag{12}$$

Here $\alpha = (3/5)\,(3\,\pi^2/2)^{2/3}$ and t_i, x_i and ν are the Skyrme force parameters. The isoscalar and isovector chemical potentials are obtained from,

$$\left.\frac{\partial E_{\text{bulk}}}{\partial A}\right|_{\mathcal{V},A_-} = \mu, \quad \left.\frac{\partial E_{\text{bulk}}}{\partial A_-}\right|_{\mathcal{V},A} = \mu_-. \tag{13}$$

The bulk equations (10), (11) and (12) allow us to derive the equimolar radius of nuclei.

Using the experimental data for the separation energy s_q for each kind of nucleons, we obtain the corresponding chemical potentials $\lambda_n = -s_n$ and $\lambda_p = -s_p$. Applying then Eqs. (5), (10) and (13), we evaluate the bulk densities ρ_V and $\rho_{-,V}$, and the surface densities $\rho_S[R]$ and $\rho_{-,S}[R]$. Note, that the square brackets in $\rho_S[R]$ and $\rho_{-,S}[R]$ denote a formal dependence on the dividing radius R which is arbitrary and may not correspond to the actual physical size of a nucleus. To derive the actual (equimolar) radius R_e of a nucleus an additional condition on the location of dividing surface should be imposed. In general, the surface energy $E_S[R]$ for an arbitrary dividing surface includes the contributions from the surface tension σ and from the binding energy of particles within the surface layer (see term $\sim (\rho_S\mu + \rho_{-,S}\mu_-)$ in Eq. (3)). In agreement with Gibbs-Tolman-Widom concept, the actual equimolar radius R_e of the droplet is determined by the requirement that the contribution to $E_S[R]$ from the bulk term in Eq. (3) should be excluded from the surface energy $E_S[R]$. The last requirement can be satisfied if the following condition is fulfilled

$$\left(\rho_S\mu + \rho_{-,S}\mu_-\right)_{R=R_e} = 0\,, \tag{14}$$

where μ and μ_- are taken under the condition of Eq. (5). Eq. (14) represents the derivation of the equimolar radius R_e for an asymmetric nucleus with $N \neq Z$.

In the case of finite nuclei, we will adopt the extended Thomas-Fermi approximation for the kinetic energy density [10]

$$\epsilon_{\mathrm{kin},q}[\rho_q] = \frac{\hbar^2}{2m}\left[\frac{3}{5}\,(3\,\pi^2)^{2/3}\,\rho_q^{5/3} + \beta\,\frac{(\boldsymbol{\nabla}\rho_q)^2}{\rho_q} + \frac{1}{3}\,\nabla^2\rho_q\right] \tag{15}$$

and the effective Skyrme interaction for the potential energy. The total energy of charged nucleus is given by

$$E_{\mathrm{tot}}\{\rho_q, \boldsymbol{\nabla}\rho_q\} = E_{\mathrm{kin}}\{\rho_q, \boldsymbol{\nabla}\rho_q\} + E_{\mathrm{Sk}}\{\rho_q, \boldsymbol{\nabla}\rho_q\} + E_{\mathrm{C}}\{\rho_p\}, \tag{16}$$

where $E_{\mathrm{Sk}}\{\rho_q, \boldsymbol{\nabla}\rho_q\}$ is the potential energy of Skyrme interaction which includes the gradient dependent terms $\sim \boldsymbol{\nabla}\rho_q$:

$$E_{\mathrm{Sk}}\{\rho_q, \boldsymbol{\nabla}\rho_q\} = \int d\,\boldsymbol{r}\;\epsilon_{\mathrm{Sk}}[\rho_q, \boldsymbol{\nabla}\rho_q], \tag{17}$$

$\epsilon_{\mathrm{Sk}}[\rho_q, \boldsymbol{\nabla}\rho_q]$ is the density of the potential energy of Skyrme interaction and $E_{\mathrm{C}}\{\rho_p\}$ is the Coulomb energy. In our consideration, the potential energy $E_{\mathrm{Sk}}\{\rho_q, \boldsymbol{\nabla}\rho_q\}$ also includes the energy due to the spin-orbit interaction.

Following the direct variational method, we choose a trial function for $\rho_q(\boldsymbol{r})$ as a power of the Fermi function for $\rho_q(\boldsymbol{r})$ given by, see also Ref. [6],

$$\rho_q(\boldsymbol{r}) = \rho_{0,q}\left[1 + \exp\left(\frac{r - R_q}{a_q}\right)\right]^{-\eta_q}, \tag{18}$$

where $\rho_{0,q}$, R_q, a_q and η_q are the unknown variational parameters. Considering the asymmetric nuclei with $X = (N - Z)/A \ll 1$, we will introduce the isotopic particle densities, namely the total density $\rho_{0,+} = \rho_{0,n} + \rho_{0,p}$ and the neutron excess density $\rho_{0,-} = \rho_{0,n} - \rho_{0,p}$ with $\rho_{0,-} \ll \rho_{0,+}$.

The profile functions $\rho_+(r)$ and $\rho_-(r)$ have to obey the condition that the numbers of neutrons and of protons are conserved. For the ground state of nucleus, the unknown parameters $\rho_{0,\pm}, R_q, a_q$ and η_q and the total energy E_{tot} itself can be obtained from the variational principle

$$\delta(E - \lambda_n N - \lambda_p Z) = 0, \tag{19}$$

where the variation with respect to all possible small changes of $\rho_{0,\pm}, R_q, a_q$ and η_q is assumed. The Lagrange multipliers λ_n and λ_p are the chemical potentials of the neutrons and the protons, respectively, and both of them are fixed by the condition that the number of particles is conserved.

III. EQUATION OF STATE OF FINITE NUCLEI AND POLARIZATION EFFECT

The introduction of a sharp (non-diffuse) equimolar surface obviates the ambiguities in the derivation of the pressure, the incompressibility and the equation of state for finite systems with a finite diffuse layer of the surface. In particular, using the concept of equimolar radius R_e, the total energy (1) of a finite nucleus can be written in the following form of Weizsäcker mass formula,

$$\begin{aligned} E_{\mathrm{tot}}(\rho_0, A, X)/A \\ &= e_0(\rho_0) + b_{\mathrm{S}}(\rho_0)A^{-1/3} \\ &+ \left[b_{\mathrm{V,sym}}(\rho_0) + b_{\mathrm{S,sym}}(\rho_0)\, A^{-1/3}\right]X^2 \\ &+ E_C(\rho_0, A, X)/A, \end{aligned} \tag{20}$$

where $e_0(\rho_0)$ is the bulk energy of a symmetric nuclear matter, $b_{\mathrm{S}}(\rho_0)$ is the surface energy coefficient, $b_{\mathrm{V,sym}}(\rho_0)$ is the volume part of symmetry energy, $b_{\mathrm{S,sym}}(\rho_0)$ is its surface part and

$$\rho_0(R_e) = A\,(3/4\pi)R_e^{-3}. \tag{21}$$

The Coulomb energy $E_C(\rho_0, A, X)$ can be written as

$$E_C(\rho_0, A, X) = \alpha_C(\rho_0)(1 - X)^2 A^{5/3} + O(A^{4/3}), \tag{22}$$

$$\alpha_C(\rho_0) = \frac{3}{20}e^2\left(\frac{4\pi\rho_0}{3}\right)^{1/3}.$$

The structure of the total energy given by Eq. (20) is similar to the semiempirical mass formula

which describes the average changes in nuclear binding energy with the mass number. However, in contrast to the mass formula, the bulk density ρ_0 and the asymmetry parameter X are not necessarily at equilibrium. The asymmetry term $\sim X^2$ includes both the volume, $b_{\mathrm{V,sym}}(\rho_0)$, and the surface, $b_{\mathrm{S,sym}}(\rho_0)$, contributions. The surface symmetry term $b_{\mathrm{S,sym}}(\rho_0)\, A^{-1/3}X^2$ appears in the advanced mass formula by Myers and Swiatecki [11,12] and it is currently employed in the description of surface properties and isovector excitations in finite nuclei, see e.g. Refs. [13,14].

Similarly to a classical liquid, the particle density ρ_0 in Eq. (20) is r-independent and the evaluation of the pressure $P(\rho_0)$ and thereby the equation of state can be obtained as in classical case [8]. In the two-component nuclei, the form of the EOS is different for the isobaric case (fixed A and different X) and isotopic case (fixed Z and different X). In the isobaric case, the EOS is derived as

$$P_A(\rho_0, X) = -\frac{\partial E_{\mathrm{tot}}(\rho_0, A, X)}{\partial V}\Big|_{A,X} = \rho_0^2 \frac{\partial E_{\mathrm{tot}}(\rho_0, A, X)/A}{\partial \rho_0}\Big|_{A,X}, \tag{23}$$

where $E_{\mathrm{tot}}(\rho_0, A, X)$ is given by Eq. (20) with <u>fixed</u> A. In isotopic case, the EOS is given by

$$P_Z(\rho_0, X) = -\frac{\partial E_{\mathrm{tot}}(\rho_0, Z, X)}{\partial V}\Big|_{Z,X} = \rho_0^2 \frac{\partial E_{\mathrm{tot}}(\rho_0, Z, X)/A}{\partial \rho_0}\Big|_{Z,X}, \tag{24}$$

where $E_{\mathrm{tot}}(\rho_0, Z, X)$ is given by Eq. (20) with $A = 2\,Z\,(1-X)^{-1}$ and <u>fixed</u> Z.
For a given bulk density ρ_0, one can derive the isobaric beta-stability line $X = X^*(A, \rho_0)$ by the condition

$$\frac{\partial E_{\mathrm{tot}}(\rho_0, A, X)}{\partial X}\Big|_{A, X=X^*} = 0. \tag{25}$$

Near the beta-stability line, the total energy (20) is written up to the order $(X - X^*)^2$ as

$$\begin{aligned} E_{\mathrm{tot}}(\rho_0, A, X) = {} & E_{\mathrm{tot}}(\rho_0, A, X^*) \\ & + \left[b_{\mathrm{V,sym}}(\rho_0)A + b_{\mathrm{S,sym}}(\rho_0)\, A^{2/3}\right. \\ & \left. - \alpha_C(\rho_0)A^{5/3}\right](X - X^*)^2. \end{aligned} \tag{26}$$

The isotopic beta-stability line $X = X^*(Z, \rho_0)$ is obtained from,

$$\frac{\partial E_{\mathrm{tot}}(\rho_0, Z, X)}{\partial X}\Big|_{Z, X=X^*} = 0 \tag{27}$$

The derivation of non-equilibrium $\rho_0(R_e)$, Eqs. (20) and (21), and the corresponding EOS requires model assumptions. One of the appropriate models is the semiclassical ETF approximation which allows us to evaluate the nucleon density distribution $\rho_q(\boldsymbol{r})$ with a finite diffuse layer and the corresponding chemical potential λ_q [5]. The calculation of the bulk density ρ_0 and the equimolar radius R_e can be then performed by using the procedure described in Sect.

II. In Fig. 1 we show the isobaric equation of state $P_A(\rho_0, X)$ for the nucleus ^{208}Pb. Note, that in agreement with the general definition of Eq. (20), the pressure $P_A(\rho_0, X)$ includes (i) the A- and X-independent bulk pressure $P_{\rm vol}(\rho_0)$ caused by the bulk energy of a symmetric nuclear matter $e_0(\rho_0)$, (ii) the surface (capillary) pressure, $P_{A,\rm capil}(\rho_0, X) \sim A^{-1/3}$, (iii) the contribution from the symmetry energy, $P_{A,\rm sym}(\rho_0, X) \sim X^2$ and (iv) the Coulomb force contribution $P_{A,\rm C}(\rho_0, X)$

$$P_A(\rho_0, X) = P_{\rm vol}(\rho_0) + P_{A,\rm capil}(\rho_0, X) + P_{A,\rm sym}(\rho_0, X) + P_{A,\rm C}(\rho_0, X). \tag{28}$$

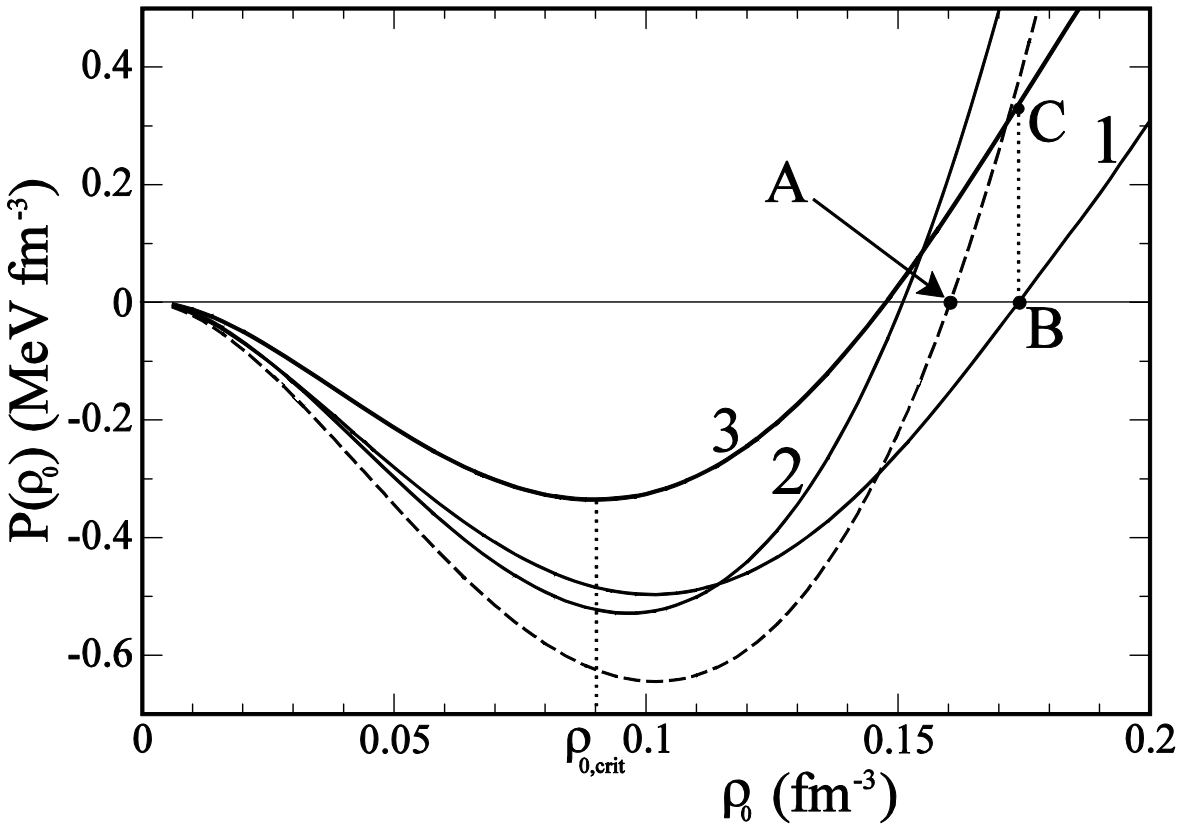

Fig. 1. Equation of state for the nucleus ^{208}Pb. The calculation was performed for **SkM*** interaction [15]. Dashed line is the EOS for the symmetric nuclear matter $\boldsymbol{P_{\rm vol}(\rho_0)}$, solid line 1 is for $\boldsymbol{P_{\rm vol}(\rho_0) + P_{\rm capil}(\rho_0, X)}$, solid line 2 is for $\boldsymbol{P_{\rm vol}(\rho_0) + P_{\rm C}(\rho_0, X)}$ and solid line 3 is the total pressure $\boldsymbol{P_A(\rho_0, X)}$ of Eq. (28).

In agreement with Eq. (23) and the equilibrium condition

$$\left.\frac{\partial E_{tot}(\rho_0, A, X)}{\partial \rho_0}\right|_{\rho_0=\rho_{0,\rm eq}} = 0, \tag{29}$$

the ground state of the nucleus is achieved at $P_A(\rho_0 = \rho_{0,\rm eq}, X) = 0$. Using the SkM* [15]

nucleon-nucleon interaction we present the results for the equation of state (EOS) for the nucleus $^{208}\mathrm{Pb}$ in Fig. 1. As seen from Fig. 1, the inclusions of the surface (capillary) term $P_{\mathrm{capil}}(\rho_0, X)$ shifts the equilibrium point to a larger values of $\rho_{0,\mathrm{eq}}$ (point B in Fig.1) with respect to the one in a nuclear matter (point A in Fig.1). Note that the capillary pressure $P_{A,\mathrm{capil}}(\rho_0, X)$ is connected to the surface tension coefficient $\sigma(A, X)$ by the Laplace relation [16]

$$P_{A,\mathrm{capil}}(\rho_0, X) = \frac{2\sigma(A, X)}{R_s}, \tag{30}$$

where R_s is the radius of tension (Laplace radius). The value of $P_{A,\mathrm{capil}}(\rho_0, X)$ is manifested by the straight dotted line BC in Fig. 1. The action of the Coulomb pressure $P_{A,\mathrm{C}}(\rho_0, X)$ is opposite to the capillary pressure $P_{A,\mathrm{capil}}(\rho_0, X)$ and shifts the equilibrium point to the smaller values of $\rho_{0,\mathrm{eq}}$.

The radius R_s is shifted with respect to the equimolar radius R_e by a small value $\xi = R_e - R_s$ (Tolman length [3]) which is caused by the finite diffuse layer in a nucleus [4,7,9]. Note also that the Tolman length ξ regulates the approach of the surface tension coefficient $\sigma(A, X)$ to the planar limit σ_∞ [4,17] in a semi-infinite system,

$$\sigma(R_e) = \sigma_\infty \left(1 - \frac{2\xi}{R_e} + \mathcal{O}(R_e^{-2})\right). \tag{31}$$

The use of the Gibbs-Tolman equimolar radius R_e allows us to provide a more realistic procedure for the extraction of the nuclear surface tension coefficient from the experimental data. Note, that the equimolar radius R_e determines the equimolar surface area $S_e = 4\pi R_e^2$ in absence of a diffuse layer. This fact gives the possibility to evaluate both the surface energy E_{S_e} and the surface tension coefficient $\sigma(A, X) = E_{S_e}/S_e$. The surface energy E_{S_e} is obtained by use the experimental value of nuclear binding energy E_{exp} and the earlier derived bulk energy E_{bulk} of nuclear matter, see Eq. (10). Namely,

$$E_{S_e} = E_{\mathrm{exp}} - E_C - E_{\mathrm{bulk}}. \tag{32}$$

The Coulomb energy E_C is subtracted from the value of binding energy E_{exp} because of the derivation of the nuclear matter energy E_{bulk} does not include the Coulomb energy contribution. Using the experimental data within the wide interval of mass number $40 \leq A \leq 220$ and the corresponding values of equimolar radii, one can establish the following A-expansion for the surface tension coefficient

$$\sigma(A, X^*) = \frac{E_{S_e}}{S_e} = \sigma_0 + \frac{\sigma_1}{A^{1/3}}, \tag{33}$$

$$\sigma_0 = (0.98 \pm 0.03)\ \mathrm{MeV\ fm^{-2}}, \quad \sigma_1 = (0.75 \pm 0.16)\ \mathrm{MeV\ fm^{-2}}.$$

The numerical result of Eq. (33) leads to the following value for the Tolman length ξ in nuclei

$$\xi = (-0.41 \pm 0.07)\ \text{fm}. \tag{34}$$

Note that both values of σ_0 and σ_1 can be derived also from the capillary pressure $P_{A,\text{capil}}(\rho_0, X)$ in Fig. 1. The corresponding values of σ_0 and σ_1 are close to those given in Eq. (33).

In Fig. 1, the minimum of the pressure $P_A(\rho_0, X)$ is located at $\rho_0 = \rho_{0,\text{crit}}$. The nucleus becomes unstable within the spinodal instability region $\rho_0 < \rho_{0.\text{crit}}$, where the incompressibility coefficient

$$K_A(A,X) = 9\,\frac{\partial P_A(\rho_0,X)}{\partial \rho_0}\Big|_{A,X} = 9\,\rho_0^2\,\frac{\partial^2 E_{tot}(\rho_0,X)/A}{\partial \rho_0^2}\Big|_{A,X} \tag{35}$$

is negative $K_A(A,X) < 0$. In accordance with Eqs. (28) and (35), the incompressibility coefficient $K_A(A,X)$ includes the volume (nuclear matter) contribution K_{NM}, the surface term $K_{\text{surf}}(A,X)$, the term $K_{\text{sym}}(A,X)$ due to the symmetry energy and the Coulomb force contribution term, $K_{\text{C}}(A,X)$. Namely,

$$K_A(A,X) = K_{NM} + K_{\text{surf}}(A,X) + K_{\text{sym}}(A,X) + K_{\text{C}}(A,X). \tag{36}$$

The equimolar radius R_e is A-dependent. In general, the variation of the equimolar radius R_e with the nucleon number A is caused by two factors. There is the simple variation term of $R_e \propto A^{1/3}$ (see Fig. 5) and an additional term which occurs due to the polarization effect in nuclei away from the beta-stability line because of the neutron excess $N - Z$. Considering the polarization effect, we will expand the total energy of Eq. (20), $E_{\text{tot}}(\rho_0, A, X)/A$, around the equilibrium bulk density $\rho_{0,\text{eq}}$. By keeping only terms quadratic in $\delta\rho_0 = \rho_0 - \rho_{0,\text{eq}}$ we rewrite Eq. (20) as,

$$E_{\text{tot}}(\rho_0,A,X)/A = E_{\text{tot}}(\rho_{0,\text{eq}},A,X^*)/A + \frac{K_A(A,X^*)}{18\rho_{0,eq}^2}(\rho_0-\rho_{0,\text{eq}})^2 + \frac{P_{A,sym}(\rho_{0,eq},X^*)}{\rho_{0,eq}^2}(X-X^*)^2(\rho_0-\rho_{0,\text{eq}}). \tag{37}$$

where

$$P_{A,\text{sym}}(\rho_0) = \rho_0^2\,\frac{\partial}{\partial\rho_0}\big[b_{\text{V,sym}}(\rho_0) + b_{\text{S,sym}}(\rho_0)\,A^{-1/3} - \alpha_C(\rho_0)A^{2/3}\big]. \tag{38}$$

For an arbitrary fixed value of X, the equilibrium density $\rho_{0,X}$ is derived by the condition

$$\frac{\partial}{\partial\rho_0}E_{\text{tot}}(\rho_0,A,X)/A\Big|_{A,\rho_0=\rho_{0,X}} = 0. \tag{39}$$

Using Eqs. (37) and (39), one obtains the polarization effect on the particle density beyond the beta-stability line

$$\rho_{0,X} = \rho_{0,\mathrm{eq}}(X^*) - 9\frac{P_{A,sym}(\rho_{0,eq}, X^*)}{K_A(A, X^*)}(X - X^*)^2. \quad (40)$$

In Fig. 2 we have plotted the partial pressure $P_{A,\mathrm{sym}}(\rho_0, X^*)$ versus the bulk density ρ_0 (partial equation of state) for the nucleus ^{208}Pb, obtained using the SkM* [15], Sly230b [18] and KDE0v1 [19] Skyrme interactions. The dashed vertical line shows the position $\rho_0/\rho_{0,\mathrm{crit}} \approx 0.6$ of the spinodal instability border. On the left side of this line the nucleus is unstable with respect to the bulk density variations.

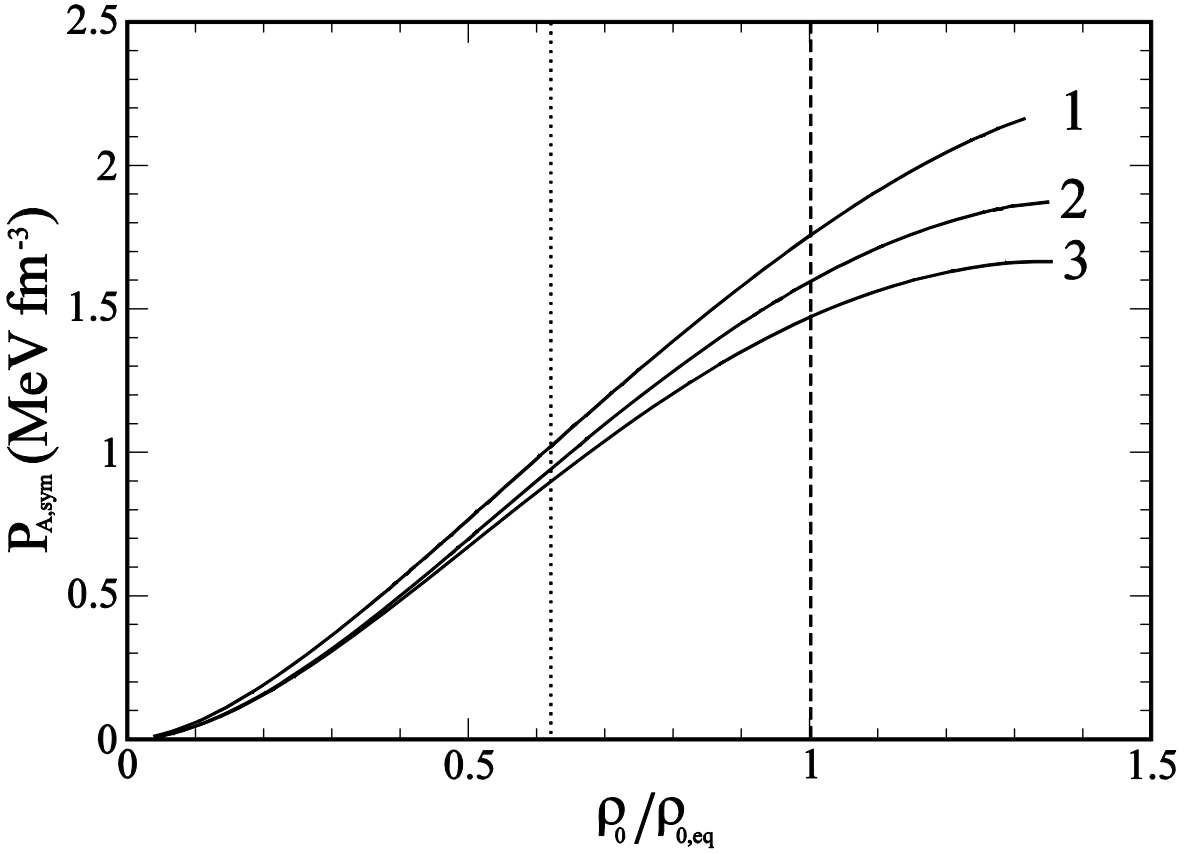

Fig. 2. The partial pressure $\boldsymbol{P_{A,\mathrm{sym}}}$ for the nucleus ^{208}Pb calculated for different parametrization of the Skyrme interactions**:** KDE0v1 [19] - solid line 1, SLy230b [18] - solid line 2 and SkM* [15] - solid line 3. The dotted vertical line is the mark for the spinodal instability border and the dashed line is for the equilibrium density.

As seen from Fig. 2, the equilibrium value of the partial pressure $P_{A,\mathrm{sym}}(\rho_{0,\mathrm{eq}})$ is positive and thereby $\rho_{0,X} < \rho_{0,\mathrm{eq}}$, see also Refs. [20,21]. The partial pressure $P_{A,\mathrm{sym}}$ is rather sensitive to the Skyrme interaction parametrization (see results for the SkM*, SLy230b and KDE0v1 in Fig. 2). The polarization effect influences the equimolar radius R_e also. The final result reads

$$R_e(A,X) = R_e^*(A,X^*)\left(1 + \frac{1}{3}\frac{P_{A,sym}(\rho_{0,eq},X^*)}{K_A(A,X^*)\rho_{0,eq}}(X-X^*)^2\right) \quad (41)$$

The magnitude of the polarization effect on the equimolar radius R_e can be also seen in Fig. 3 where we compare the A-dependence of the equimolar radius $R_e = R_e^*(A,X^*)$ for the nuclei on the beta stability line in the presence of the partial polarization pressure, $P_{A,\mathrm{sym}}(\rho_{0,eq},X^*)$ (solid

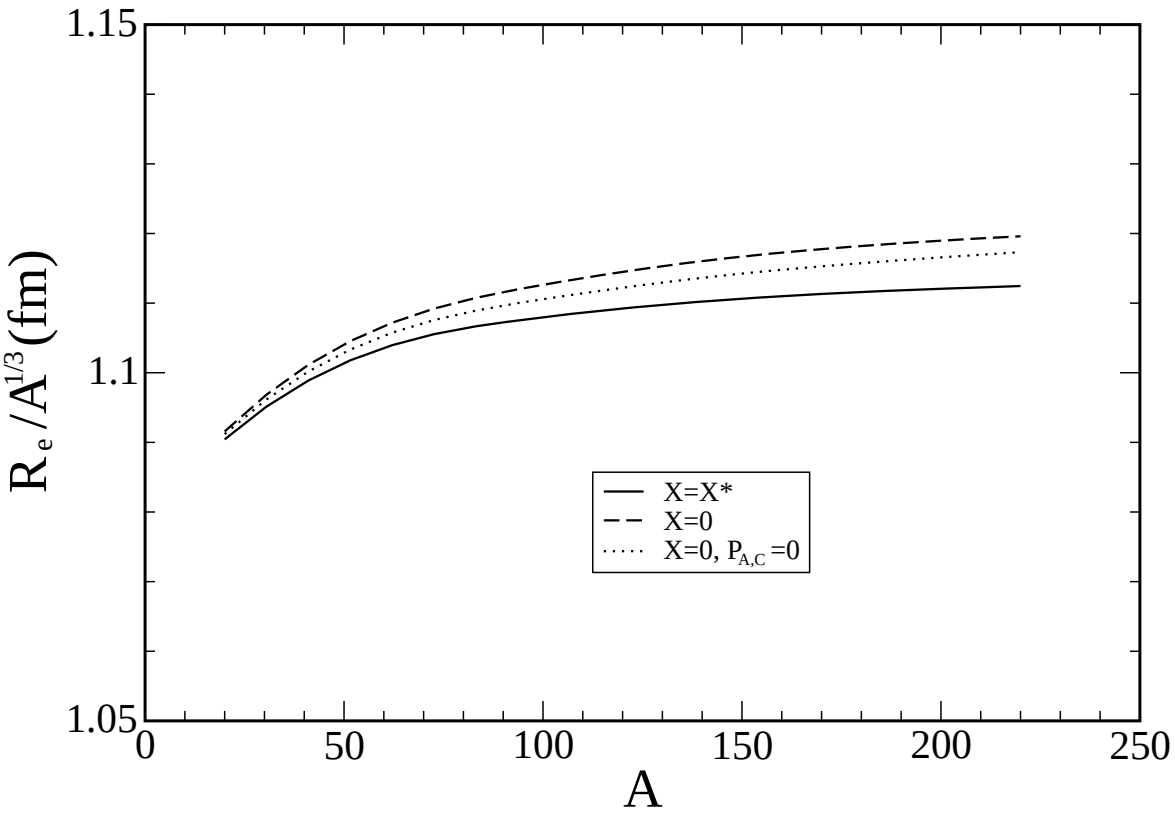

Fig. 3. Dependence of equimolar radius $\boldsymbol{R_e = R_e^*(A,X^*)}$ on the mass number $\boldsymbol{A}$ on the beta-stability line in presence of the polarization effect (solid line). The dashed line is the equimolar radius $\boldsymbol{R_e(A,X=0)}$ where the polarization effect is absent. The dotted line is obtained by elimination of the Coulomb force polarization effect, see Eq. (46). The calculations were performed for the SkM* [15] interaction.

Considering the symmetric nuclei, with $X = 0$, one can estimate the polarization effect due only to the Coulomb interaction. Using Eq. (20) for the symmetric case $N = Z$, we write

$$E_{\mathrm{tot}}(\rho_0,A,X=0)/A = e_0(\rho_0) + b_{\mathrm{S}}(\rho_0)A^{-1/3} + \alpha_C(\rho_0)A^{2/3}, \quad (42)$$

where ρ_0 is related to the equimolar radius R_e as in Eq. (21). Assuming that $\tilde{\rho}_{0,\mathrm{eq}}$ is the equilibrium density for the uncharged liquid drop, we will expand the total energy of Eq. (42)

around the equilibrium density $\tilde{\rho}_{0,\mathrm{eq}}$ as

$$E_{\mathrm{tot}}(\rho_0, A, X=0)/A = E_{\mathrm{tot}}(\tilde{\rho}_{0,\mathrm{eq}}, X = 0)/A + \frac{K_A(A, X=0)}{18\tilde{\rho}_{0,eq}^2}(\rho_0 - \tilde{\rho}_{0,\mathrm{eq}})^2 + \frac{P_{A,C}(\tilde{\rho}_{0,eq})}{\tilde{\rho}_{0,eq}^2}(\rho_0 - \tilde{\rho}_{0,\mathrm{eq}}). \quad (43)$$

where,

$$P_{A,\mathrm{C}}(\rho_0) = \rho_0^2 \frac{\partial}{\partial \rho_0}\alpha_C(\rho_0)A^{2/3}, \quad (44)$$

is the Coulomb force pressure. The equilibrium density $\rho_{0,\mathrm{eq}}$ of a symmetric nucleus in presence of Coulomb forces is obtained from the condition

$$\frac{\partial}{\partial \rho_0}E_{\mathrm{tot}}(\rho_0, A, X=0)/A\Big|_{A,\rho_0=\rho_{0,\mathrm{eq}}} = 0. \quad (45)$$

Using Eqs. (37), (39) and (45), one obtains the polarization effect on the particle density caused by Coulomb forces for symmetric nuclei with $N = Z$

$$\rho_{0,\mathrm{eq}} = \tilde{\rho}_{0,\mathrm{eq}} - 9\frac{P_{A,C}(\tilde{\rho}_{0,eq})}{K_A(A, X=0)}. \quad (46)$$

The Coulomb force pressure is positive $P_{A,\mathrm{C}}(\rho_0) > 0$, see Eqs. (22) and (44), and thereby the polarization effect, which is caused by the Coulomb forces, decreases the bulk density $\rho_{0,\mathrm{eq}}$, i.e., increases the nuclear equimolar radius R_e of Eq. (21). The corresponding numerical result is shown in Fig. 3 as the dotted line.

IV. NUCLEAR RADII

Using the experimental values [22] of the chemical potentials λ and λ_- for the arbitrary dividing radius R and the fixed asymmetry parameter X, one can evaluate the volume part of equilibrium energy $E_{\mathcal{V}}$ from Eq. (10), and the particle numbers in the volume, $A_{\mathcal{V}} = 4\pi\rho R^3/3$ and $A_{-,\mathcal{V}} = 4\pi\rho_- R^3/3$, and in the surface, $A_{\mathcal{S}} = 4\pi\rho_{\mathcal{S}} R^2$ and $A_{-,\mathcal{S}} = 4\pi\rho_{-,\mathcal{S}} R^2$, particle numbers. All these evaluated values depend on the radius R of the dividing surface and the asymmetry parameter X.

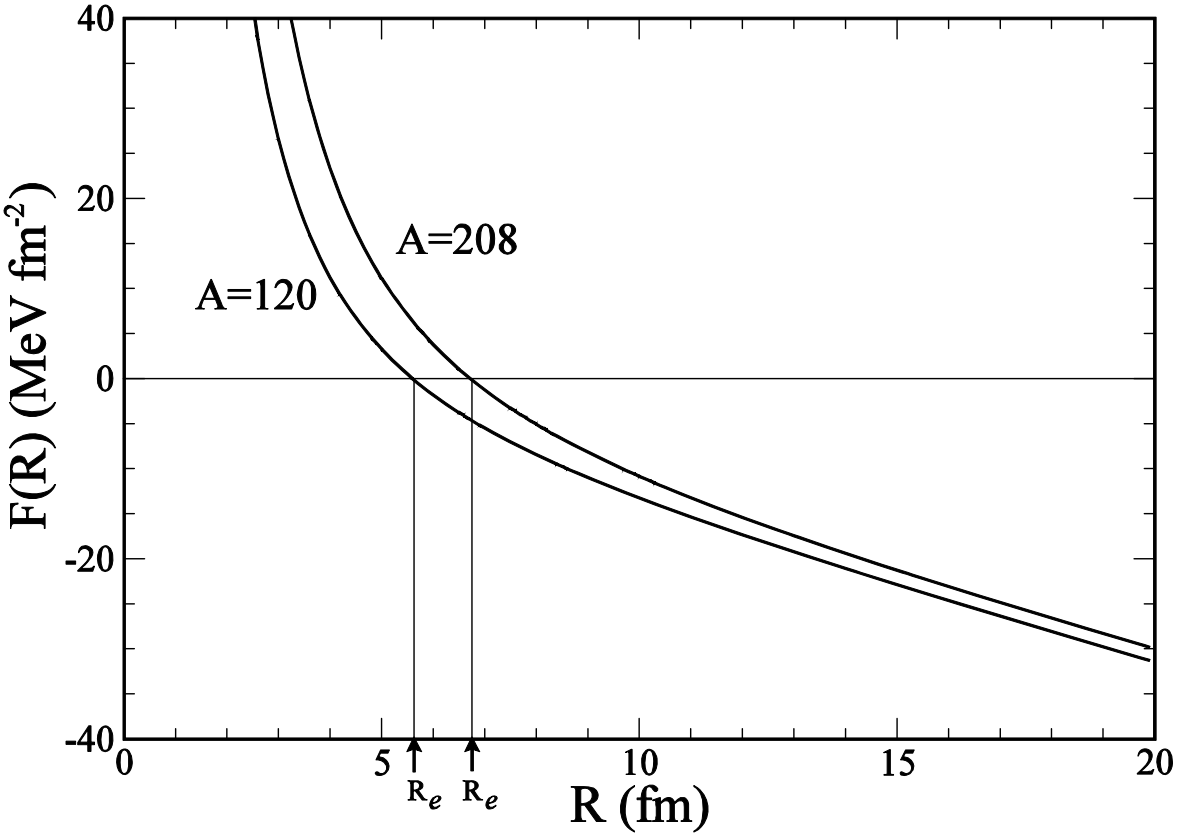

Fig. 4. Specific surface particle density $\boldsymbol{F(R) = -(\varrho_S \mu + \varrho_{-,S} \mu_-)}$ versus dividing radius $\boldsymbol{R}$ for nuclei with $\boldsymbol{A = 208}$ and $\boldsymbol{A = 120}$. The calculation was performed using the SkM* interaction [15]. $\boldsymbol{R_e}$ denotes the equimolar radius where $\boldsymbol{F(R) = 0}$.

As noted above, the actual physical radius R_e of the nucleus is determined by the condition (14), i.e., by the requirements that the contribution to E_S from the bulk binding energy (term $\sim (\rho_S \lambda + \rho_{-,S} \lambda_-)$ in Eq. (3)) should be excluded from the surface energy E_S. In Fig. 4 we represent the results of the calculation of the specific surface particle density $F(R) = -(\rho_S \lambda + \rho_{-,S} \lambda_-)$ as a function of the radius R of the dividing surface. The equimolar dividing radius R_e in Fig. 4 defines the physical size of the sharp surface droplet and the surface at which the surface tension is applied, i.e., the equimolar surface where Eq. (14) is fulfilled.

The evaluated equimolar radius R_e does not necessary obey the saturation condition $R_e \sim A^{1/3}$. This reflects the fact that the experimental data for the chemical potentials λ and λ_- used in our calculations includes the quantum shell effects, the pairing correlation effects, etc. In Fig. 5 we have plotted the evaluated equimolar radii R_e for some nuclei. The solid line shows the average behavior $R_e = r_0 A^{1/3}$.

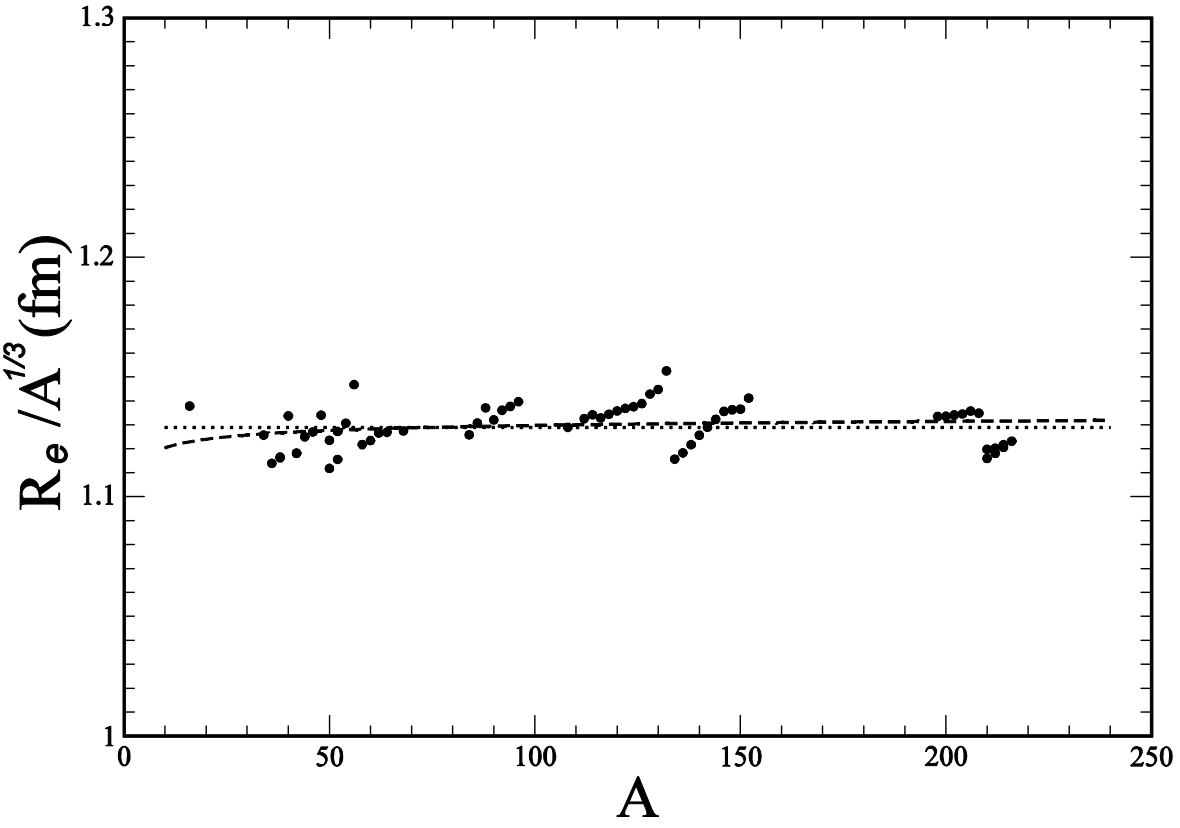

Fig. 5. $\boldsymbol{A}$-dependence of equimolar nuclear radius $\boldsymbol{R_e(A)}$. Solid points were obtained within the Gibbs-Tolman procedure where the experimental values for the nucleon chemical potential were used and the dashed line is for the corresponding averaged values of equimolar radii $\boldsymbol{R_e}$. Dotted line is for $\boldsymbol{R_e = 1.13\, A^{1/3}}$ fm. The SkM* interaction [15] was used.

We point out that the average interparticle distance r_0 is slightly A-dependent (see dashed line in Fig. 5)

$$r_0 \approx \left(1.14 - \frac{0.04}{A^{\frac{1}{3}}}\right) \text{ fm.} \tag{47}$$

The non-monotonic behavior of the nuclear equimolar radii $R_e(A)$ is caused by the quantum shell fluctuations, the pairing effects, etc., which are manifested in the experimental values of the chemical potentials λ_n and λ_p.

V. SKIN AND HALO EFFECTS – ISOVECTOR SHIFT OF RADII

The above described procedure can be used to derive the partial equimolar radii $R_{e,q}(A)$ separately for neutrons, $q = n$, and for protons, $q = p$, and the corresponding nucleon rms radii

$\sqrt{\langle r_q^2 \rangle}$. Using the experimental values of the chemical potentials λ_n and λ_p of actual nuclei and Eqs. (10) - (13), one can derive the partial bulk densities ρ_n and ρ_p. Evaluating then the partial surface nucleon densities

$$\rho_{n,s}[R] = \frac{N}{4\pi R^2} - \frac{1}{3}\rho_n R\,, \quad \rho_{p,s}[R] = \frac{Z}{4\pi R^2} - \frac{1}{3}\rho_p R \tag{48}$$

and applying the condition of Eq. (14), we find the partial equimolar radii $R_{e,q}(A)$. Considering the rms radii

$$\sqrt{\langle r_q^2 \rangle} = \sqrt{\int d\boldsymbol{r}\, r^2\, \rho_q(r) / \int d\boldsymbol{r}\, \rho_q(r)} \tag{49}$$

in presence of the finite diffuse layer, we will introduce the dispersion of the surface layer [1]

$$b_q = \sqrt{\int_0^\infty d\, r\, g_q(r)(r - \overline{r}_q)^2}, \tag{50}$$

where

$$g_q(r) = -d\, f_q(r)/dr, \qquad \overline{r}_q = \int_0^\infty d\, r\, r\, g_q(r)$$

and $f_q(r) = \rho_q(r)/\rho_{0,q}$ is the profile function of the nucleon density.

In the case of the Fermi- like profile function $f(r)$ of Eq. (18), one obtains

$$b_q = a_q \sqrt{[2\kappa_1(\eta_q) - \kappa_0^2(\eta_q)]}, \tag{51}$$

where the coefficients $\kappa_i(\eta)$ are given by [6]

$$\kappa_i(\eta) = \int_0^\infty d\, x\, x^i \left[(1 + e^x)^{-\eta} - (-1)^i (1 - (1 + e^{-x})^{-\eta})\right]. \tag{52}$$

Finally, the nucleon rms radii read, see also [1],

$$\sqrt{\langle r_q^2 \rangle} \approx \sqrt{3/5} R_{e,q} \left[1 + \frac{5}{2}\left(\frac{b_q}{R_{e,q}}\right)^2\right]. \tag{53}$$

Note that the surface layer correction $\sim b_q^2$ to the rms radii in Eq. (53) can exceed the value of about 10% in light and middle nuclei. We point out also that the rms radii $\sqrt{\langle r_q^2 \rangle}$ of Eq. (53) as well as the equimolar radii $R_{e,q}(A)$ contain the shell fluctuations, see Fig. 5.

The partial equimolar radius $R_{e,q}$ and the corresponding rms radii $\sqrt{\langle r_q^2 \rangle}$ can be evaluated numerically from Eqs. (10) - (13) and (53) using the chemical potentials λ_n and λ_p of actual nuclei. As an example we will show the result for the ^{208}Pb nucleus. In this case, using the variational procedure of Eq. (19) and trial function for $\rho_q(\boldsymbol{r})$ of Eq. (18), we obtain for the SkM*

interaction $a_n = 0.723$ fm, $a_p = 0.618$ fm, $\eta_n = 4.048$ and $\eta_p = 5.158$. Using the average interparticle distance r_0 from Eq. (47) and Eq. (53), one obtains for the mass rms radius $\sqrt{\langle r^2 \rangle} = 5.447$ fm which agrees with experimental data $\sqrt{\langle r^2 \rangle}|_{\text{exp}} = (5.579 \pm 0.025)$ fm [27]. In Fig. 6, we show also the evaluated values of the proton rms radius $\sqrt{\langle r_p^2 \rangle}$ for the Na isotopes.

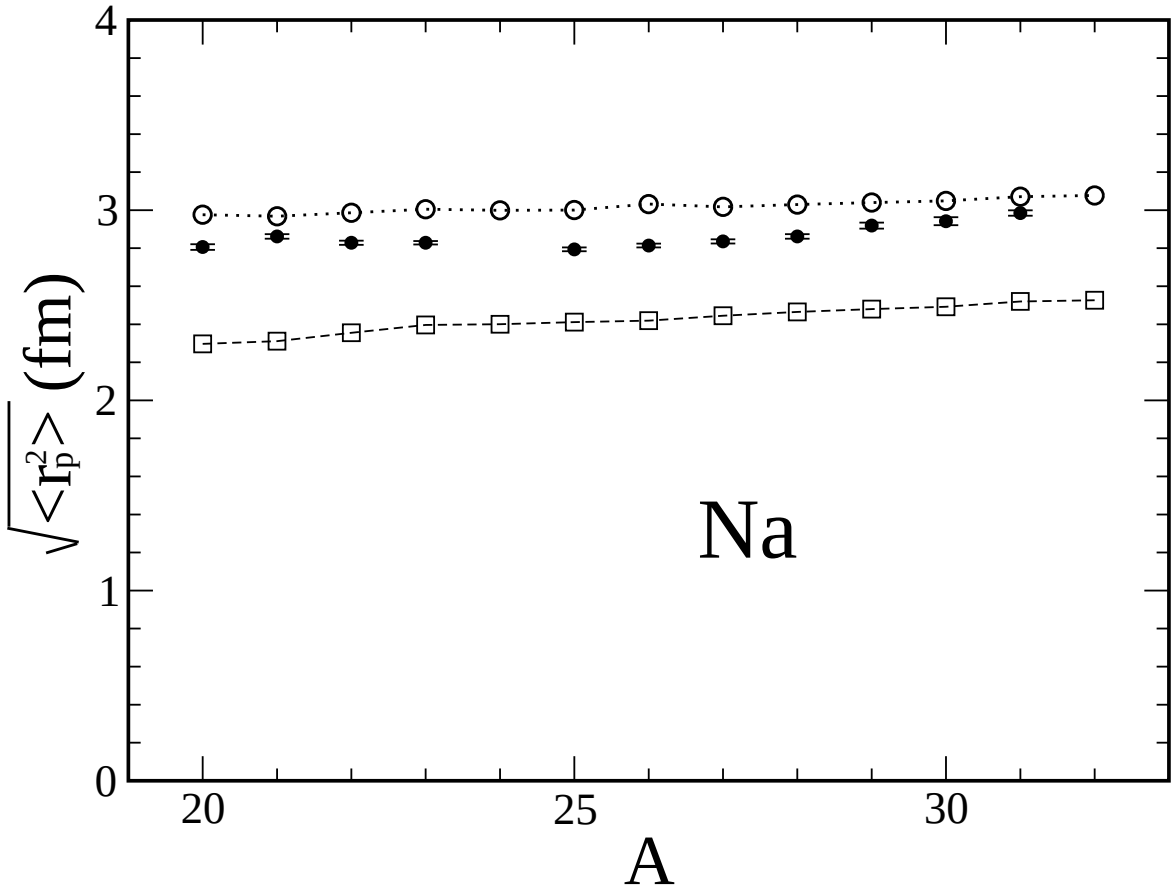

Fig. 6. The rms radius of proton distribution in Na isotopes obtained by use of Eq. (53). The dotted line with open circels was obtained with surface layer correction $\sim \boldsymbol{b_q^2}$ and the dashed line with open squares is for $\boldsymbol{b_q^2 = 0}$. Here and below the experimintal data were taken from Ref. [24]. The SkM* interaction [15] was used.

Evaluating the isovector shift of particle density ρ_-, one can determine the neutron-skin

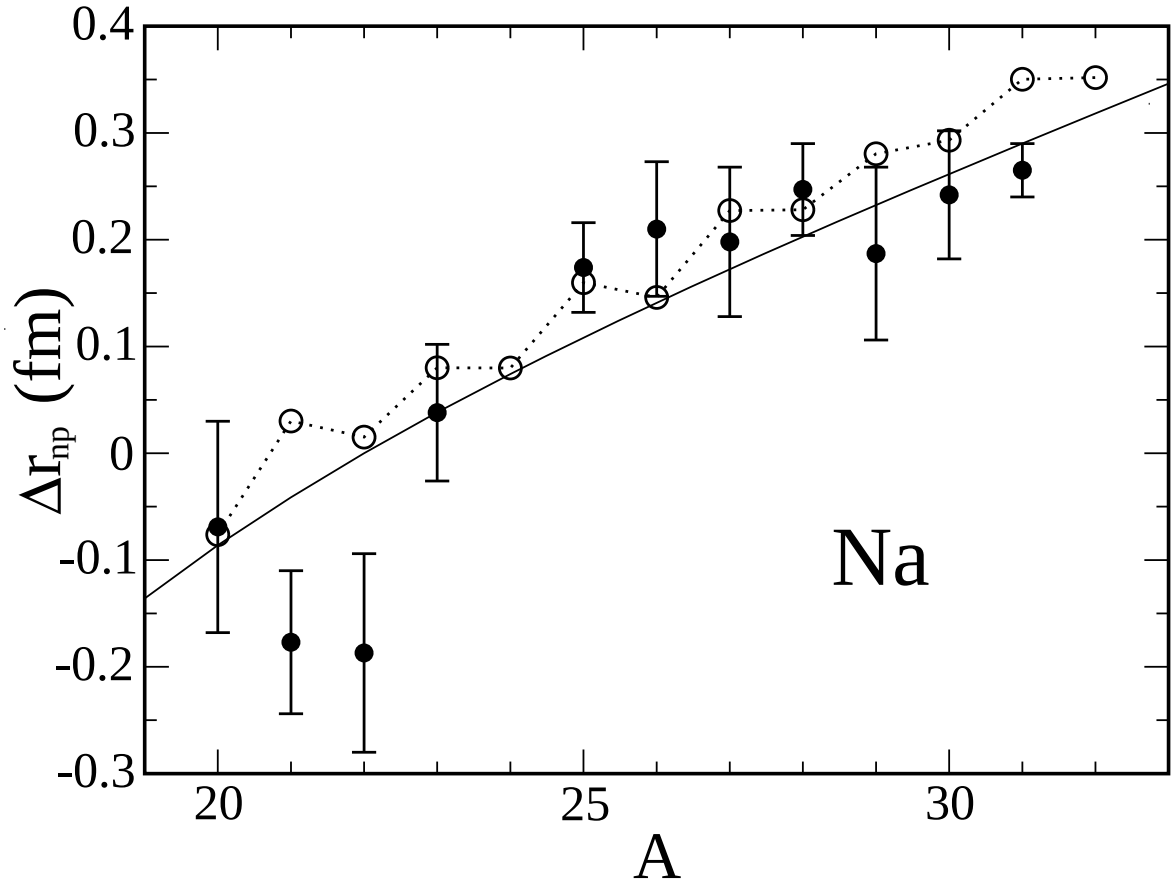

Fig. 7. Isovector shift of nuclear rms radius $\boldsymbol{\Delta r_{np}} = \sqrt{\langle r_n^2 \rangle} - \sqrt{\langle r_p^2 \rangle}$ in Na isotopes. The solid points are the experimental data [24], the open circles (connected by dotted line) have been obtained using the Gibbs-Tolman approach described in text and the solid line is obtained using the extended Thomas-Fermi approximation with the **SkM*** Skyrme interaction [15], see Ref. [6].

As seen from Figs. 7, 8 and 9, the Gibbs-Tolman-Widom concept of the sharp equimolar surface allows one to describe the fine non-monotonic structure of the nucleon rms radius and

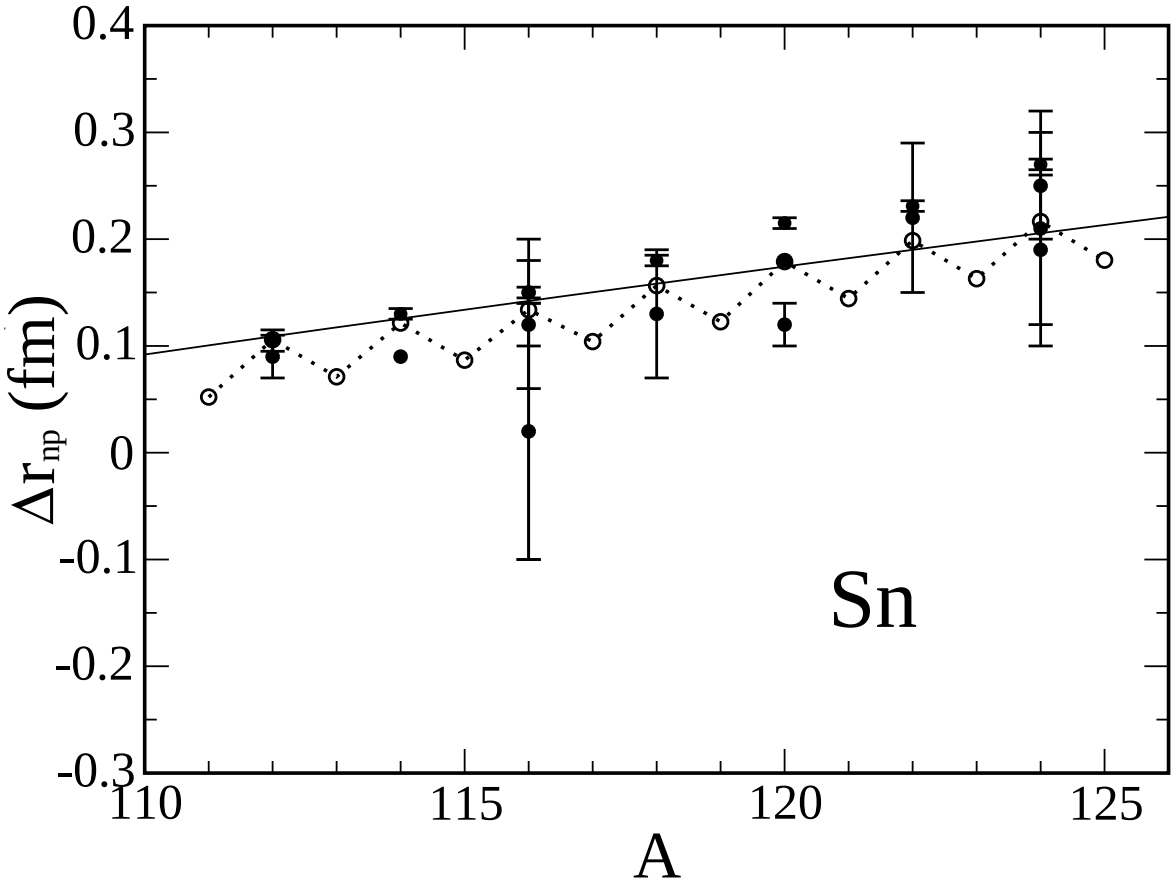

Fig. 8. The same as in Fig. 7 but for Sn isotopes. The data were taken from Refs. [23,25,26].

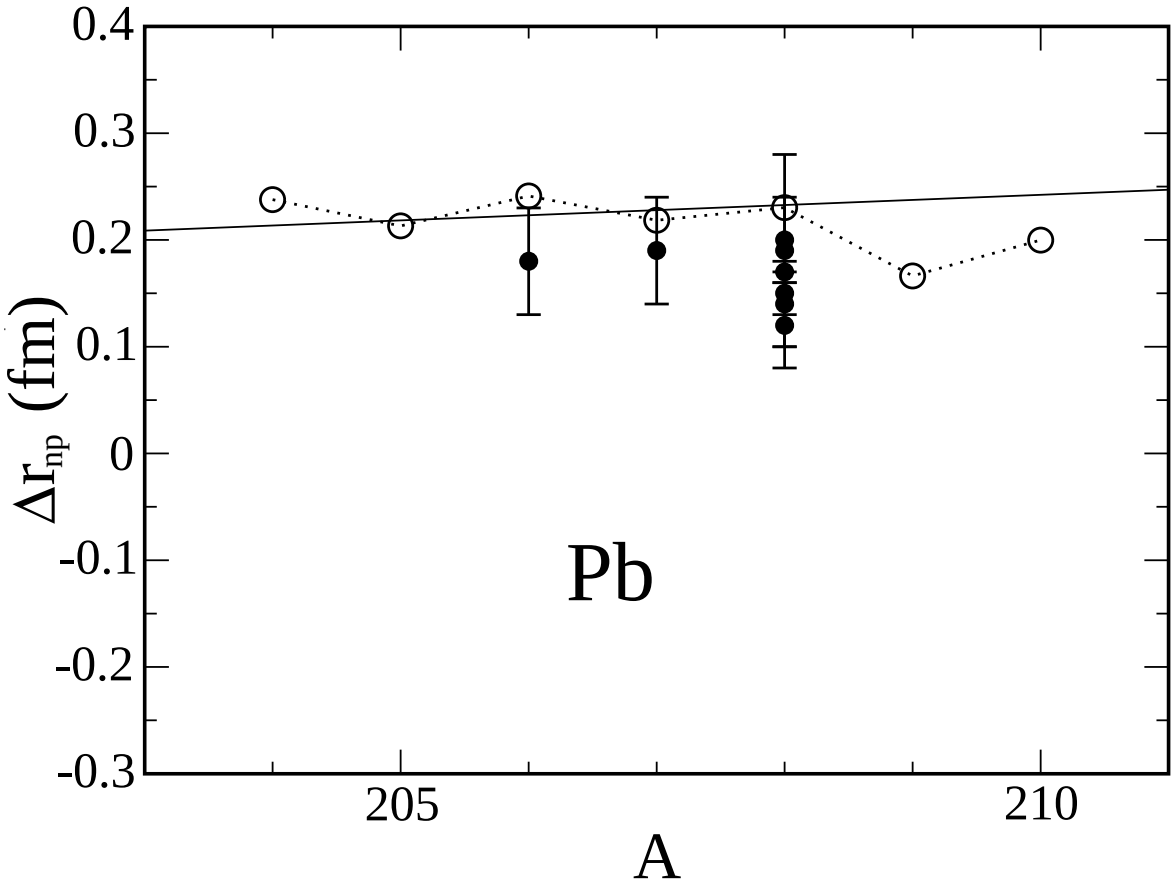

Fig. 9. The same as in Fig. 7 but for Pb isotopes. The experimental data were taken from Refs. [27,28,29].

In general, the value of the isovector shift Δr_{np} is the sum of two contributions: the one, $\Delta r_{np,R}$, is due to the different radii (skin effect) and the other, $\Delta r_{np,a}$, is due to the different shape (surface layer) of neutron and proton distributions (halo effect) , see also Refs. [25,26,30,31,32],

$$\Delta r_{np} = \Delta r_{np,R} + \Delta r_{np,a}, \tag{54}$$

Both values of $\Delta r_{np,R}$ and $\Delta r_{np,a}$ can be obtained from Eq. (53) and are given by following expressions

$$\Delta r_{np,R} \approx \sqrt{\frac{3}{5}}\left[1 - \frac{5}{2}\left(\frac{b}{R_e}\right)^2\right]\Delta_{R,e} \tag{55}$$

and

$$\Delta r_{np,a} \approx 5\sqrt{\frac{3}{5}}\frac{b}{R_e}\Delta_b. \tag{56}$$

Here, $\Delta_{R,e} = R_{e,n} - R_{e,p}$, $b = (b_n + b_p)/2$ and $\Delta_b = b_n - b_p$ are the parameters of neutron skin.

Expressions (54), (55) and (56) dissect the structure of the neutron-skin thickness Δr_{np}. In Fig. 10 we have plotted the values of $\chi = \Delta r_{np,a}/\Delta r^*_{np,a}$ (the value $\Delta r^*_{np,a}$ is taken on the beta-stability line at $X = X^*$) versus the deviation $\Delta X = X - X^*$ from the beta-stability line

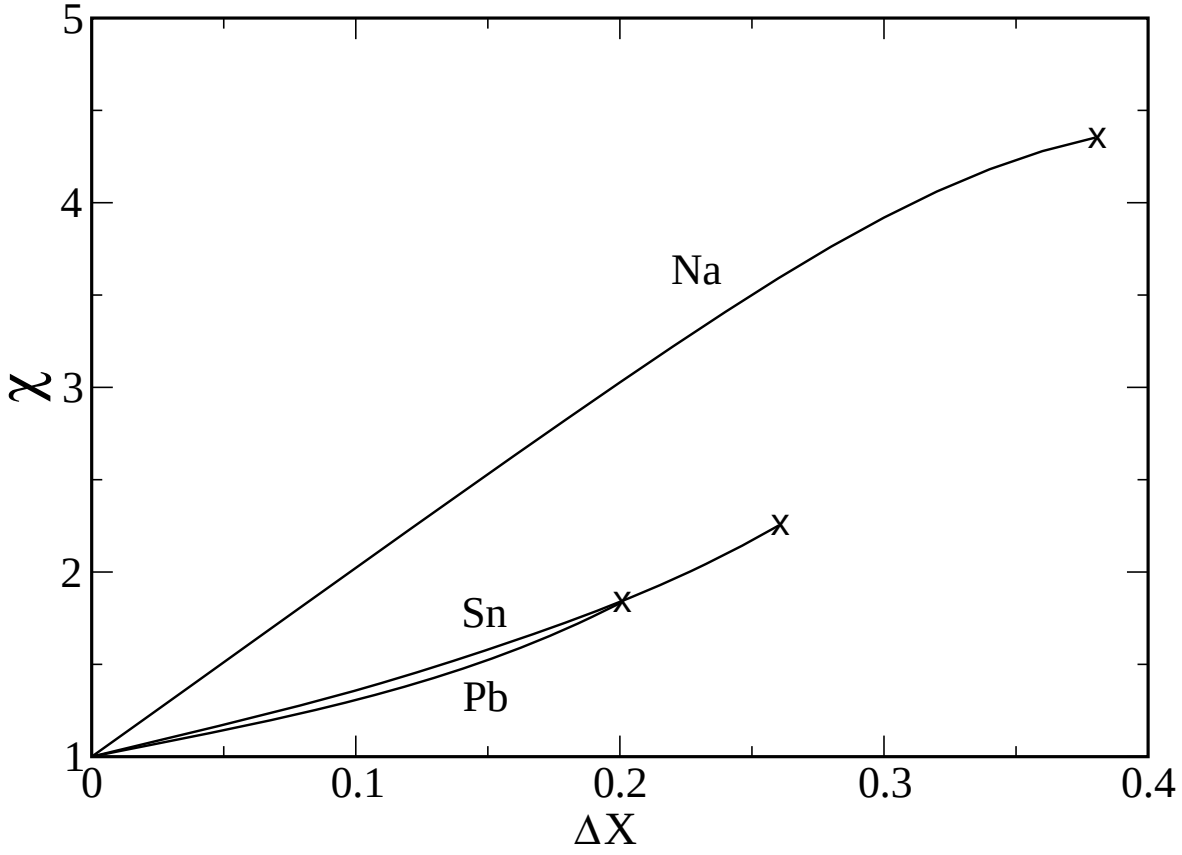

Fig. 10. The ratio $\boldsymbol{\chi = \Delta r_{np,a}/\Delta r^*_{np,a}}$ versus the deviation $\boldsymbol{\Delta X = X - X^*}$ from the beta-stability line for isotopes of nuclei Na, Sn and Pb. The calculations have been performed performed using the **SkM*** interaction [15] and the Weizsecker's parameter $\boldsymbol{\beta = 1/9}$ (see Eq. (15)). The crosses at the end of lines denote the neutron drip-line which is derived by the condition $\lambda_n = 0$.

The numerical results for $\Delta r_{np,a}$ are sensitive to the choice of the gradient corrections to the kinetic energy density $\epsilon_{\mathrm{kin},q}[\rho_q]$ (see the term with the parameter β in Eq. (15)). In Fig. 10, we have used the empirical value for the Weizsäcker's parameter $\beta = 1/9$. Note also that evaluating the skin parameter $\Delta_{R,e}$ in Eq. (55) we have used the Gibbs-Tolman-Widom procedure

which is described in Sec. II. As can be seen from Fig. 10, the relative contribution of the shape (halo) effect, i.e. $\Delta r_{np,a}$, to the isotopic shift of radii Δr_{np} is more evident in the light nuclei. As it can be expected, the ratio $\Delta r_{np,a}/\Delta r^{*}_{np,a}$ increases for nuclei away from the beta-stability line, i.e., for the neutron rich isotopes.

VI. CONCLUSIONS

We have applied the approach proposed earlier by Gibbs-Tolman-Widom for a classical liquid drop in presence of the liquid-vapor interface to the derivation of actual size of a nucleus in presence of finite surface diffuse layer. The basic idea of the Gibbs-Tolman-Widom approach is the introduction of a sharp dividing surface $\mathcal{S}$ [2,3,4]. The dividing surface is arbitrary but located within the surface diffuse layer. The actual (physical) equimolar surface and thereby the actual nuclear surface are fixed by the requirement that the contribution to the surface energy $E_{\mathcal{S}}[R] \sim A^{2/3}$ from the bulk energy $E_{\rm bulk} \sim A$ should be eliminated, see Eq. (14). The bulk density ρ_0 of neutrons and protons inside the sharp equimolar surface is obtained using the experimental data for the separation energy s_q for each kind of nucleons.

The Gibbs-Tolman-Widom conception of sharp equimolar surface allows one to derive the nuclear volume and, as a consequence, the pressure $P(\rho_0)$ and the equation of state for finite nuclei. In our consideration, we have performed the calculations of well-defined equation of state for spherical nuclei and some nuclear characteristics such as the nuclear radius, the surface tension, the pressure, etc. Our numerical calculations are based on the direct variational method, the extended Thomas-Fermi approximation and the effective Skyrme nucleon-nucleon interaction. Applying the Gibbs-Tolman-Widom approach, we redefine the surface and symmetry energies. Note that we do not use the traditional leptodermous approximation and evaluate the Coulomb energy taking into consideration the finite diffuse layer of the proton distribution.

Performing the analysis of the equation of state $P = P(\rho_0)$, we have extracted from $P(\rho_0)$ the partial contributions which occur due to the different sources: the A- and X-independent bulk pressure $P_{\rm vol}(\rho_0)$ caused by the bulk energy of a symmetric nuclear matter; the surface (capillary) pressure, $P_{A,\rm capil}(\rho_0, X) \sim A^{-1/3}$; the contribution from the symmetry energy, $P_{A,\rm sym}(\rho_0, X) \sim X^2$ and the Coulomb force contribution $P_{A,\rm C}(\rho_0, X)$. The corresponding numerical results are shown in Fig. 1 for the ^{208}Pb nucleus. The inclusion of surface (capillary) term $P_{\rm capil}(\rho_0, X)$ shifts the equilibrium point $\rho_{0,\rm eq}$ to larger values with respect to the ones in a nuclear matter. Note also that the capillary pressure $P_{A,\rm capil}(\rho_0, X)$ is connected to the surface tension coefficient

$\sigma(A,X)$ by the classical Laplace relation. The action of the Coulomb pressure $P_{A,\mathrm{C}}(\rho_0,X)$ is opposite to the capillary pressure $P_{A,\mathrm{capil}}(\rho_0,X)$ and shifts the equilibrium point to the smaller values of $\rho_{0,\mathrm{eq}}$.

The use of the Gibbs-Tolman-Widom equimolar radius R_e allowed us to give a more realistic procedure for an extraction of the nuclear surface tension coefficient from the experimental data. The equimolar radius R_e determines the equimolar surface area S_e in absence of a diffuse layer. This fact allows us to evaluate both the surface energy E_{S_e} and the surface tension coefficient $(A,X) = E_{S_e}/S_e$. Using the experimental data within the wide interval of mass number $40 \le A \le 220$ and the corresponding values of equimolar radii, we have established the following A-expansion for the surface tension coefficient $\sigma(A,X^*) = \sigma_0 + \sigma_1 A^{-1/3}$ with $\sigma_0 = (0.98 \pm 0.03)$ MeV fm^{-2} and $\sigma_1 = (0.75 \pm 0.16)$ MeV fm^{-2}. The obtained result for the curvature correction $\sigma_1 A^{-1/3}$ allows one to estimate the Tolman length ξ in nuclei which is $\xi = (-0.41 \pm 0.07)$ fm.

We have evaluated the partial pressure $P_{A,\mathrm{sym}}(\rho_0,X)$ caused by the symmetry energy. The partial pressure $P_{A,\mathrm{sym}}(\rho_0,X)$ induces the polarization effect on the particle density $\rho_{0,X}$ beyond beta-stability line. We have shown that the partial pressure $P_{A,\mathrm{sym}}(\rho_{0,\mathrm{eq}})$ is positive and reduces the particle density $\rho_{0,X}$ with respect the corresponding equilibrium density $\rho_{0,\mathrm{eq}}$ on the beta-stability line. The partial pressure $P_{A,\mathrm{sym}}$ and the polarization effect are rather sensitive to the Skyrme interaction parametrization (see results for the SkM*, SLy230b and KDE0v1 in Fig. 2). We point out that the evaluated equimolar radius R_e of the nuclei does not necessary obey the saturation condition $R_e = r_0 A^{1/3}$. That is caused by the fact that we use the experimental data for the chemical potentials to derive the bulk density within the equimolar surface in agreement with the Gibbs-Tolman-Widom method. The corresponding experimental chemical potentials (separation energy of nucleons) include the quantum shell effects, the pairing correlation effects, etc., and give rise to the non-monotonic behavior of the nuclear equimolar radii $R_e(A)$ in Fig. 5. Note also that the average interparticle distance r_0 becomes slightly A-dependent (see dashed line in Fig. 5).

Using the partial equimolar radii $R_{e,q}(A)$ separately for both kind of nucleons, we have evaluated the corresponding nucleon rms radii $\sqrt{\langle r_q^2 \rangle}$ and the neutron-skin thickness $\Delta r_{np} = \sqrt{\langle r_n^2 \rangle} - \sqrt{\langle r_p^2 \rangle}$. The evaluated values of the proton rms radius $\sqrt{\langle r_p^2 \rangle}$ for the Na isotopes (see Fig. 6) show a slightly non-monotonic behavior of $\sqrt{\langle r_p^2 \rangle}$ which is caused by the above mentioned

fluctuations of $R_{e,p}$. Note also the presence of the significant shift up of the proton rms $\sqrt{\langle r_p^2 \rangle}$ (compare dashed and dotted lines in Fig. 6) caused by the surface layer corrections. The influence of the pairing and shell effects on the neutron-skin thickness Δr_{np} is illustrated in Figs. 7, 8 and 9 for Na, Sn and Pb isotopes. As seen from Figs. 7, 8 and 9, the Gibbs-Tolman-Widom concept of the sharp equimolar surface allows one to describe a fine non-monotonic structure of the isovector shift Δr_{np}. The saw-like behavior of Δr_{np} (see the open circles which connected by the dotted line in these figures) reflects the even-odd and shell effects in the nuclear binding energy and thereby in the nuclear radii. In general, the value of the isovector shift Δr_{np} is the sum of two contributions: the one, $\Delta r_{np,R}$, is due to the different radii (skin effect) and the other, $\Delta r_{np,a}$, is due to the different shape (surface layer) of neutron and proton distributions (halo effect). The presence of the halo effect is illustrated in Fig. 10. One can expect that the neutron halo effect appears more significantly in light nuclei far away the stability line.

VII. ACKNOWLEDGEMENTS

This work was supported in part by the National Academy of Sciences of Ukraine under grant # CO-2-14/2016 (V.M.K., S.V.L. and A.I.S.) and by the US Department of Energy under contract # DOE-FG03-93ER40773 (S.S.). S. Shlomo also thanks the Weizmann Institute for the Weston Visiting Professorship Award and the nice hospitality extended to him.

[1] W.D. Myers, Nucl. Phys. **A204**, 465 (1973).

[2] J.W. Gibbs, *Collected Works, Vol. I* (Longmans Green and Company, New York, 1928).

[3] R.C. Tolman, J. Chem. Phys. **17**, 118, 333 (1949).

[4] J.S. Rowlinson and B. Widom, *Molecular Theory of Capillarity* (Clarendon Press, Oxford, 1982).

[5] V.M. Kolomietz and A.I. Sanzhur, Eur. Phys. J. A **38**, 345 (2008).

[6] V.M. Kolomietz, S.V. Lukyanov and A.I. Sanzhur, Phys. Rev. C **85**, 034309 (2012).

[7] V.M. Kolomietz, S.V. Lukyanov and A.I. Sanzhur, Phys. Rev. C **86,** 024304, 2012.

[8] L.D. Landau and E.M. Lifshitz, *Statistical Physics* (Pergamon Press, Oxford, 1958).

[9] V.M. Kolomietz and A.I. Sanzhur, Phys. Rev. C **88**, 044316 (2013).

[10] D.A. Kirzhnitz, *Field Theoretical Methods in Many Body Systems* (Pergamon, London, 1967).

[11] W.D. Myers and W.J. Swiatecki, Ann. Phys. **55**, 395 (1969).

[12] W.D. Myers and W.J. Swiatecki, Ann. Phys. **84**, 186 (1974).

[13] P. Möller, J.R. Nix, W.D. Myers and W.J. Swiatecki, At. Data Nucl. Data Tables **59**, 185 (1995).

[14] P. Danielewicz, Nucl. Phys. **A 727**, 233 (2003).

[15] M. Brack, C. Guet, H.-B. Haakansson, Phys. Rep. **123**, 275 (1985).

[16] L. D. Landau and E. M. Lifshitz, *Fluid mechanics* (Pergamon Press, London, 1959).

[17] M.J.P. Nijmeijer, C. Bruin, A.B. van Woerkom and A.F. Bakker, J. Chem. Phys. **96**, 565 (1992).

[18] E. Chabanat, R Bonche, R Haensel, J. Meyer, and R. Schaeffer, Nucl. Phys. A635, 231 (1998).

[19] B. K. Agrawal, S. Shlomo, and V. K. Au, Phys. Rev. C **72**, 014310 (2005).

[20] K. Oyamatsu, I. Tanichata, S. Sugahara, K. Sumiyoshi and H. Toki, Nucl. Phys. **A 634**, 3 (1998).

[21] K. Oyamatsu and K. Iida, Progr. Theor. Phys. **109**, 631 (2003).

[22] G. Audi, A.H. Wapstra and C. Thibault, Nucl. Phys. **A 729**, 337 (2003).

[23] L. Ray, Phys. Rev. C **19** , 1855 (1979).

[24] T. Suzuki, H. Geissel, O. Bochkarev, *et al*., Phys. Rev. Lett. **75**, 3241 (1995).

[25] A. Trzcińska, J. Jastrzébsky, P. Lubiński, *et al*., Phys. Rev. Lett. **87**, 082501 (2001).

[26] A. Krasznahorskay, H. Akimune, A.M. van den Berg, *et al*., Nucl. Phys. **A731**, 224 (2004).

[27] V.E. Starodubsky, N.M. Hintz, Phys. Rev. C **49**, 2118 (1994).

[28] S. Karataglidis, K. Amos, B.A. Brown, P.K. Deb, Phys. Rev. C **65**, 044306 (2002).

[29] B.C. Clark, L.J. Kerr, S. Hama, Phys. Rev. C **67**, 054605 (2003).

[30] S. Mizutori, J. Dobaczewski, G.A. Lalazissis, W. Nazarewicz and P.-G. Reinhard, Phys. Rev. C **61**, 044326 (2000).

[31] M. Warda, X. Viñas, X. Roca-Maza and M. Centelles, Phys. Rev. C **81**, 054309 (2010).

[32] M. Centelles, X. Roca-Maza, X. Viñas and M. Warda, Phys. Rev. C **82**, 054314 (2010).

FIGURE CAPTIONS

Fig. 1. Equation of state for the nucleus ^{208}Pb. The calculation was performed for **SkM*** interaction [15]. Dashed line is the EOS for the symmetric nuclear matter $\boldsymbol{P_{vol}(\rho_0)}$, solid line 1 is for $\boldsymbol{P_{vol}(\rho_0) + P_{capil}(\rho_0, X)}$, solid line 2 is for $\boldsymbol{P_{vol}(\rho_0) + P_C(\rho_0, X)}$ and solid line 3 is the total pressure $\boldsymbol{P_A(\rho_0, X)}$ of Eq. (28).

Fig. 2. The partial pressure $\boldsymbol{P_{A,sym}}$ for the nucleus ^{208}Pb calculated for different parametrization of the Skyrme forces: KDE0v1 [19] - solid line 1, SLy230b [18] - solid line 2 and – SkM* [15] - solid line 3. The dotted vertical line is the mark for the spinodal instability border and the dashed line is for the equilibrium density.

Fig. 3. Dependence of equimolar radius $\boldsymbol{R_e = R_e^*(A, X^*)}$ on the mass number $\boldsymbol{A}$ on the beta-stability line in presence of the polarization effect (solid line). The dashed line is the equimolar radius $\boldsymbol{R_e(A, X = 0)}$ where the polarization effect is absent. The dotted line is obtained by elimination of the Coulomb force polarization effect, see Eq. (46). The calculations were performed for the SkM* [15] interaction.

Fig. 4. Specific surface particle density $\boldsymbol{F(R) = -(\varrho_S \mu + \varrho_{-,S} \mu_-)}$ versus dividing radius $\boldsymbol{R}$ for nuclei with $\boldsymbol{A = 208}$ and $\boldsymbol{A = 120}$. The calculation was performed using the SkM* interaction [15]. $\boldsymbol{R_e}$ denotes the equimolar radius where $\boldsymbol{F(R) = 0}$.

Fig. 5. $\boldsymbol{A}$-dependence of equimolar nuclear radius $\boldsymbol{R_e(A)}$. Solid points were obtained within the Gibbs-Tolman procedure where the experimental values for the nucleon chemical potential were used and the dashed line is for the corresponding averaged values of equimolar radii $\boldsymbol{R_e}$. Dotted line is for $\boldsymbol{R_e = 1.13\, A^{1/3}}$ fm. The SkM* interaction [15] was used.

Fig. 6. The rms radius of proton distribution in Na isotopes obtained by use of Eq. (53). The dotted line with open circles was obtained with surface layer correction $\sim \boldsymbol{b_q^2}$ and the dashed line with open squares is for $\boldsymbol{b_q^2 = 0}$. Here and below the experimintal data were taken from Ref. [24]. The SkM* interaction [15] was used.

Fig. 7. Isovector shift of nuclear rms radius $\boldsymbol{\Delta r_{np} = \sqrt{\langle r_n^2 \rangle} - \sqrt{\langle r_p^2 \rangle}}$ in Na isotopes. The solid points are the experimental data [24], the open circles (connected by dotted line) have been obtained using the Gibbs-Tolman approach described in text and the solid line is obtained using the extended Thomas-Fermi approximation with the **SkM*** Skyrme interaction [15], see Ref. [6].

Fig. 8. The same as in Fig. 7 but for Sn isotopes. The data were taken from Refs. [23,25,26].

Fig. 9. The same as in Fig. 7 but for Pb isotopes. The experimental data were taken from Refs. [27,28,29].

Fig. 10. The ratio $\boldsymbol{\chi = \Delta r_{np,a}/\Delta r^{*}_{np,a}}$ versus the deviation $\boldsymbol{\Delta X = X - X^{*}}$ from the beta-stability line for isotopes of nuclei Na, Sn and Pb. The calculations have been performed performed using the $\mathbf{SkM}^{*}$ interaction [15] and the Weizsecker's parameter $\boldsymbol{\beta = 1/9}$ (see Eq. (15)). The crosses at the end of lines denote the neutron drip-line which is derived by the condition $\lambda_n = 0$.